Global Health & Medicine. 2025; 7(4):315-323.
ORIGINAL ARTICLE
DOI: 10.35772/ghm.2025.01077

An evaluation of the effectiveness of 3D virtual imaging combined with intraoperative ultrasonography to guide liver staining in anatomic segmental hepatectomy

Jiafu Guan[1,2,3,§], Rongyuan Liang[1,2,3,§], Yonghai Peng[4,§], Xin Yu[1,2,3], Rongfa Yuan[1,2,3], Zhigang Hu[1,2,3], Huajun Wu[1,2,3], Binghai Zhou[1,2,3], Yumin Qiu[1,2,3], Kai Wang[1,2,3,*]

[1] Hepato-Biliary-Pancreatic Surgery Division, Department of General Surgery, The Second Affiliated Hospital of Nanchang University, Nanchang, China;
[2] Jiangxi Provincial Clinical Research Center for General Surgery Disease, Nanchang, China;
[3] Jiangxi Provincial Engineering Research Center for Hepatobiliary Disease, Nanchang, China;
[4] Department of Hepatobiliary Surgery, Mianyang Central Hospital, Mianyang, China.

Abstract: Identification of a tumor-bearing portal territory using indocyanine green (ICG) fluorescence imaging (IGFI) facilitates precise laparoscopic anatomic hepatectomy (LAH). However, it is technically challenging to perform a transhepatic portal injection of ICG or to clamp the target portal pedicle and inject ICG during LAH. Herein, we aimed to investigate the feasibility and efficacy of portal territory identification using IGFI under the combined guidance of three-dimensional (3D) virtual imaging and intraoperative ultrasound (IOUS) in LAH. We enrolled patients eligible for LAH in the current study between June 2020 and April 2023. All patients had preoperative surgical planning based on 3D virtual imaging in which the boundaries of the tumor-bearing portal territory were displayed and the predicted remnant liver volumes (PRLVs) were calculated. We then conducted ICG fluorescence liver-segment staining and LAH under the combined guidance of 3D virtual imaging and IOUS. Actual remnant liver volumes (ARLVs) were calculated using 3D virtual imaging after surgery. Of the 73 patients who achieved a valid demarcation by IGFI, 14 (19.2%) underwent hemi-hepatectomy, while 19 (26%) and 40 (54.8%) underwent sectionectomy and segmentectomy, respectively. The IGFI-identified intraoperative hepatic segment boundaries were highly matched with the boundaries of the tumor-bearing portal territory in the 3D virtual images in 72 (98.6%) patients, and we observed that the ARLVs and PRLVs were also robustly correlated ($r^2 = 0.8734$, $p < 0.0001$). In summary, 3D virtual imaging and IOUS contribute significantly to the staining and identification of a tumor-bearing portal territory and the accurate implementation of LAH.

***Keywords*:** 3D virtual imaging, Intraoperative ultrasonography, Laparoscopic anatomic hepatectomy, Indocyanine green fluorescence imaging

1. Introduction

Anatomic hepatectomy is defined as the complete removal of an anatomically and relatively independent hepatic segment or subsegment, or a combination of hepatic segments (*1*). Anatomic hepatectomy removes the lesion along with the hepatic segments of the tumor-bearing portal branch, playing an especially significant role in eradicating possible intrahepatic micrometastases; this then achieves surgical margin safety, reduces intraoperative bleeding and the incidence of perioperative biliary complications, and attenuates the risk of postoperative liver failure (*2,3*). Therefore, anatomic hepatectomy is valuable in the treatment of liver malignancies such as hepatocellular carcinoma (HCC), intrahepatic cholangiocarcinoma (ICC), and liver metastases from colon cancer (*4-6*). It is acknowledged that the identification of the tumor-bearing portal territory is essential for the precise execution of anatomic hepatectomy (*7*). Traditionally, identification of the portal territory is based on superficial markings produced by the staining of the portal branch as guided by intraoperative ultrasound (IOUS) (*8*), or by interruption of the portal pedicle that serves the segment(s) (*9*). These techniques do not offer a readily durable line of demarcation on the hepatic surface, and they often fail to stain liver segments and subsegments. In addition, the techniques do not provide clear, effective guidance with respect to

the direction of liver parenchyma dissection (*10*).

Indocyanine green (ICG) fluorescence imaging (IGFI) has been adopted widely, particularly during laparoscopic hepatectomy, in order to visualize hepatic segments by transhepatic injection of ICG into tumor-bearing or tumor-free portal branches under IOUS guidance (*i.e.*, positive staining or counterstaining), or by intravenous administration of ICG after clamping the target portal pedicle (*i.e.*, negative staining) (*11*). This technique enables the clear and persistent visualization of portal territory at the liver surface and within the hepatic parenchyma relative to conventional dye injection techniques. However, in laparoscopic hepatectomy, IOUS-guided precise puncture of the target portal branch or clamping the segmental portal pedicle remains technically challenging. For successful performance of these operations, it is crucial to establish the anatomic relationship between the tumor and the neighboring structures preoperatively and to conduct detailed preoperative planning. With the development of modern digital imaging techniques, three-dimensional (3D) virtual imaging modalities have been gradually introduced to visualize intrahepatic structures and to facilitate preoperative planning of liver resection (*12,13*). 3D virtual imaging technology provides a more intuitive, clear, and multi-angle view of the size, location, and shape of the tumor and the course of the intrahepatic vessels — as well as their spatial relationships — with significant advantages over conventional preoperative assessments. In addition, 3D virtual imaging not only enables the display and quantification of the perfusion territory of each portal branch (thus contributing to individualized hepatic segmentation, virtual hepatectomy (VH), and determination of the number of tumor-bearing portals and their specific orientations) but also allows slicing of the 3D virtual images in any plane and displaying the anatomic structures such as blood vessels and tumors on the cut surface (*14*). The cut surface in a specific plane can then be used to simulate IOUS images for quick and accurate intraoperative identification of the target portal branch. Thus, the combination of 3D virtual imaging and IOUS techniques may facilitate the puncture or clamping of target portal branches and also expedite the success of IGFI staining of the target liver segment during laparoscopic anatomic hepatectomy (LAH).

In this study, we described our experience with the co-application of 3D virtual imaging and IOUS techniques in LAH for ICG fluorescence liver-segment staining.

2. Materials and Methods

2.1. Materials

We enrolled a total of 821 patients with hepatic malignancies who underwent laparoscopic hepatectomy from June 2020 to April 2023 at the Second Affiliated Hospital of Nanchang University and from June 2022 to April 2023 at Mianyang Central Hospital. Of the 821 patients, 73 patients underwent VH preoperatively using 3D virtual imaging software, and then, they underwent LAH with tumor-bearing portal territory identification using IGFI. We analyzed 60 men and 13 women, with a median age of 62 (interquartile range, 48–68) years. Of these, 67 were diagnosed with HCC, five with ICC, and one with both HCC and ICC (Table 1 presents details of the baseline characteristics of all patients). We obtained written informed consent from all patients prior to hepatectomy. This study received the approval of Research Ethics Commission of the Second Affiliated Hospital of Nanchang University (No. 2021050) and was conducted in accordance with the Declaration of Helsinki.

2.2. Acquisition and processing of 3D virtual images

Computed tomography (CT) data were obtained using a 256-slice helical CT scanner (Brilliance iCT, Philips Medical Systems, Haifa, Israel); and the scan data requirements were arterial, portal, and delayed-phase CT images and a slice thickness of 1 mm. The 3D virtual image was reconstructed based on the preoperative CT scan data by employing CT image postprocessing software (Xudong Digital Medical Imaging Technology Co., Shenzhen, China) as follows:

i) We first imported the digital imaging and communications in medicine (DICOM) image data from the thin-layer CT scans. *ii*) The hepatic artery, hepatic vein, and portal images on two-dimensional (2D) CT images were then automatically segmented by adopting the threshold analysis algorithm, and the 3D virtual image of the intrahepatic vasculature was automatically reconstructed. *iii*) Multiple seed points were selected in the target region of the 2D image, and a region-growing algorithm and a periodic iteration-segmentation method

Table 1. Summary of characteristics of patients

Variables	Values
Age, median [IQR], years	62 [48–68]
Male, *n* (%)	60 (82.2)
Background liver	
Normal liver, *n* (%)	18 (24.7)
Chronic hepatitis, *n* (%)	55 (75.3)
Preoperative diagnosis	
HCC, *n* (%)	67 (91.8)
ICC, *n* (%)	5 (6.8)
cHCC-ICC, *n* (%)	1 (1.4)
Child-Pugh class	
A, *n* (%)	73 (100)
Tumor size, median [IQR], mm	44 [35.5–60.5]
Tumor number	
Single, *n* (%)	61 (83.6)
Multiple (≤ 3), *n* (%)	12 (16.4)

HCC: hepatocellular carcinoma, ICC: intrahepatic cholangiocarcinoma, cHCC-ICC: combined hepatocellular-hepatocellular, IQR: interquartile range.

were automatically applied to segment and reconstruct the 3D virtual images of the liver and tumor. *iv*) Finally, we calculated the territories of all tertiary portals and a portion of the quaternary portals around the tumor. The algorithm for the calculation of the portal territory was based on the Voronoi tessellation, which is bordered by a line equidistant from the surrounding vessels (*15*).

Surgeons can identify the tumor-bearing portal branch and the spatial-location relationship of the tumor with nearby portal territories through 3D virtual imaging software. We conducted VH by subtracting the tumor-bearing portal territory from the entire liver; and we calculated the predicted remnant liver volumes (PRLVs) after VH. PRLV-to-standard liver volume (SLV) ratio was calculated to ensure that the residual liver volume ratio was > 40%, and the SLV was subsequently calculated based on the Urata formula (*16*). Hepatectomy terminology was determined in accordance with the 2000 Terminology Committee of the International Hepato-Pancreato-Biliary Association (*17*), and morbidity was established in accordance with the 2009 Clavien–Dindo classification of surgical complications (*18*).

Preoperative identification of tumor-bearing portal branches by 3D virtual image software provides an anatomic basis for searching for the target portal branch. However, as the IOUS image is a 2D image, difficulties remain in accurately locating the target portal branch by directly matching it with the 3D virtual image. Thus, the 3D virtual image is cut according to the possible placement directions and angles of the IOUS. In our case, the IOUS images were also simulated using cut surfaces of 3D virtual images to reduce the difficulty of target portal branch identification under IOUS and to improve the success rate of portal puncture. The target portal branch was then identified when an IOUS image matched the simulated image. When negative staining was planned, the surgeon executed 3D virtual imaging to plan access to the target portal branch in order to reduce the difficulty of dissecting or clamping the laparoscopic tumor-bearing portal branch.

2.3. ICG fluorescence imaging system

IGF images were acquired using a fluorescence laparoscopy system (IMAGE1 S, Karl Storz SE & Co. KG, Tuttlingen, Germany). This system enables the acquisition of color images under white illumination, monochrome fluorescence images under near-infrared illumination, and fused images of pseudocolor (green) fluorescence images with white-light color images. In addition, surgeons were able to select the imaging mode displayed on the screen at any time with a button switch.

2.4. Administration of ICG for the identification of the portal territory

The IGFI technique for identifying the tumor-bearing portal territory described above was appropriately selected according to the preoperative 3D virtual image. The IOUS was used to find the target portal vein branches from the first hepatic portal towards the tumour. The target portal vein branch is identified when an image similar to the section image of the preoperative 3D visualisation image is found on the ultrasound monitor. For transhepatic portal injection of ICG, 5–10 mL of ICG (0.025 mg/mL) was injected into the portal branch under IOUS guidance without clamping the Glisson pedicle at the hepatic hilum.

For intravenous injection of ICG, 5–10 mL of ICG (0.25 mg/mL) was injected after tumor-bearing portal branch occlusion or ligation. We observed fluorescence images on the surface of the liver after ICG administration and on the cut surface of the liver when the liver parenchyma was dissected, and we recorded them by applying a fluorescence laparoscopy system.

Compared with other methods, negative staining is more likely to be applied for hemi-hepatectomy, lobectomy, or left-sided segmentectomy because the origin of the secondary branches of the Glisson pedicle is principally located outside the liver or close to the surface of the liver near the hilum (*9*), allowing it to be clamped without or with only a slight dissection of the liver parenchyma. In contrast, positive staining or counterstaining tends to be used in resections, wherein the hilar separation is considered difficult due to technical reasons or in right-sided hepatic segmental resections, as a majority of the tumor-bearing portal branches are deep within the liver. In addition, a combination of these techniques may be used in complex cases. In the following sections, we describe representative cases with technical details.

2.5. Positive staining technique (Case 1)

We planned LAH for a 4.9-cm-diameter HCC, and the functional reserve was normal with a Child-Pugh class of A. The preoperative 3D virtual image showed that the HCC was located at segment VIII (S8), but the portal vein trunk of S8 was very short and divided into ventral (P8v) and dorsal (P8d) branches after entering the S8 segment (Figure 1, A and B). In this situation, as direct injection of P8 tended to cause ICG reflux resulting in staining failure, we decided on P8v and P8d injections. The IOUS images of punctures at P8v and P8d were simulated preoperatively using 3D virtual imaging technology (Figure 1, C and D), and we rapidly found IOUS images that matched the simulated images intraoperatively and identified the target portal branches (Figure 1, E and F). P8v and P8d were thus successfully punctured and subsequently injected with ICG diluted with sterile water. The S8 was ultimately completely removed (Figure 1, G and H).

2.6. Counterstaining technique (Case 2)

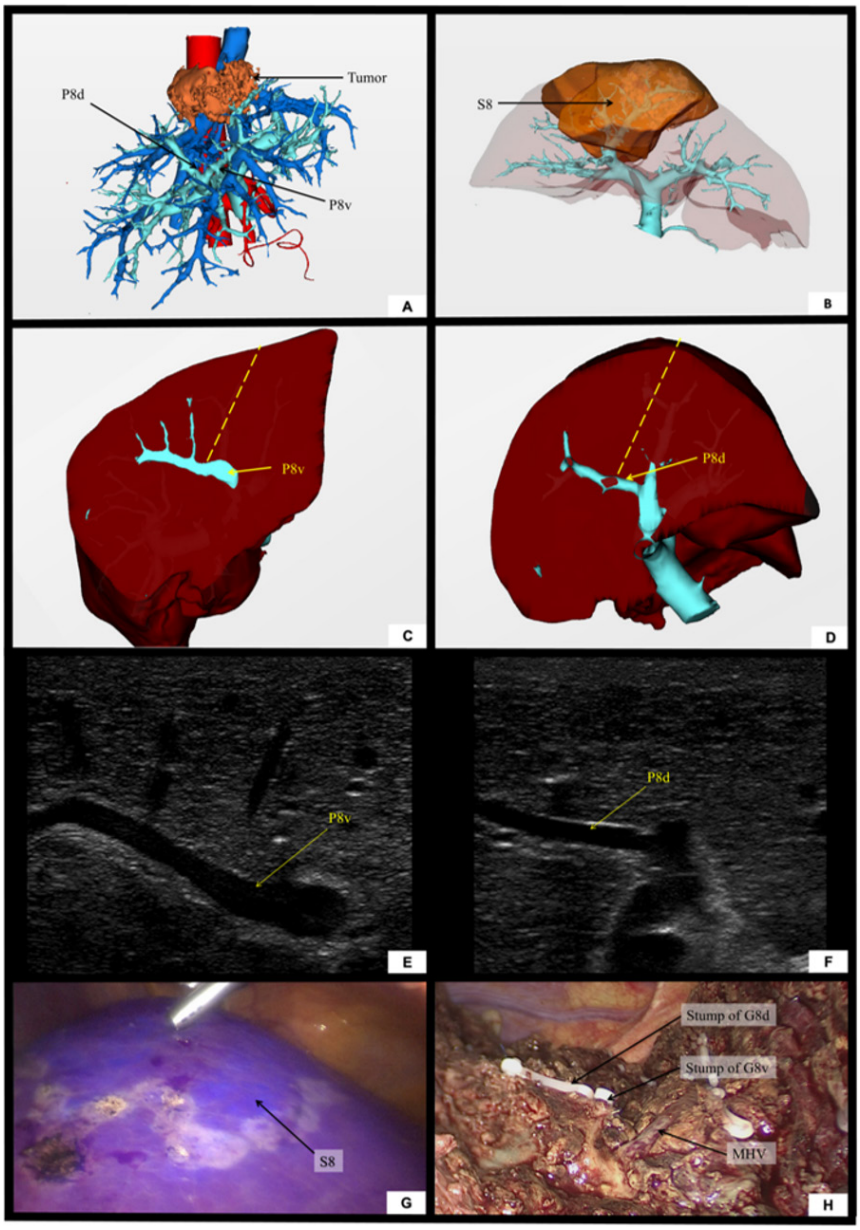

Figure 1. Positive staining. (A) 3D image shows that the tumor was located at segment VIII (S8), with P8 divided into the dorsal branch (P8d) and ventral branch (P8v). **(B)** 3D image shows the perfusion territory of P8. **(C, D)** IOUS images during the puncture of P8v and P8d were simulated using 3D visualization technology. **(E, F)** IOUS images during the puncture of P8v and P8d. **(G)** ICG fluorescence imaging clearly shows S8 as fluorescing. **(H)** Cut surface of the liver after S8 resection using positive staining. A portion of the MHV is visible in the cut surface. IOUS, intraoperative ultrasound; ICG, indocyanine green; MHV, middle hepatic vein.

When the tumor-bearing portal branch is obstructed by a portal cancer thrombus, the tumor-bearing portal territory can be identified by counterstaining, as first introduced by Takayama *et al.* in 1991 (*19*); this could alternatively be applied when the tumor-bearing portal is too thin and difficult to puncture. In our case, the tumor-bearing portal territory showed a fluorescence-deficient region, and the nearby tumor-free portal territory was displayed as a fluorescent area upon fluoroscopic laparoscopy after portal injection of ICG. LAH was planned for an HCC with a diameter of 8.7 cm. The 3D virtual image depicted the tumor as located at segment V (S5) and the ventral subsegments of segment VI (S6v); several small portal branches also flowed into S5, and the portal branching into the ventral side of S6 was thin (Figure 2, A and B). Since this situation increased the difficulty of portal puncture, we planned to puncture the portal branches flowing to segment VIII (S8) and the dorsum of S6 (S6d). We then simulated the IOUS images of the punctures at P8 and P6d preoperatively using 3D visualization technology (Figure 2, C and D). P6d and P8 were then successfully identified and punctured under IOUS guidance (Figure 2, E and F), and the tumor-bearing portal territory appeared as a fluorescence-deficient region. A complete resection of the S6v and S5 was thus achieved, whereas the territory supplied by the P6d was

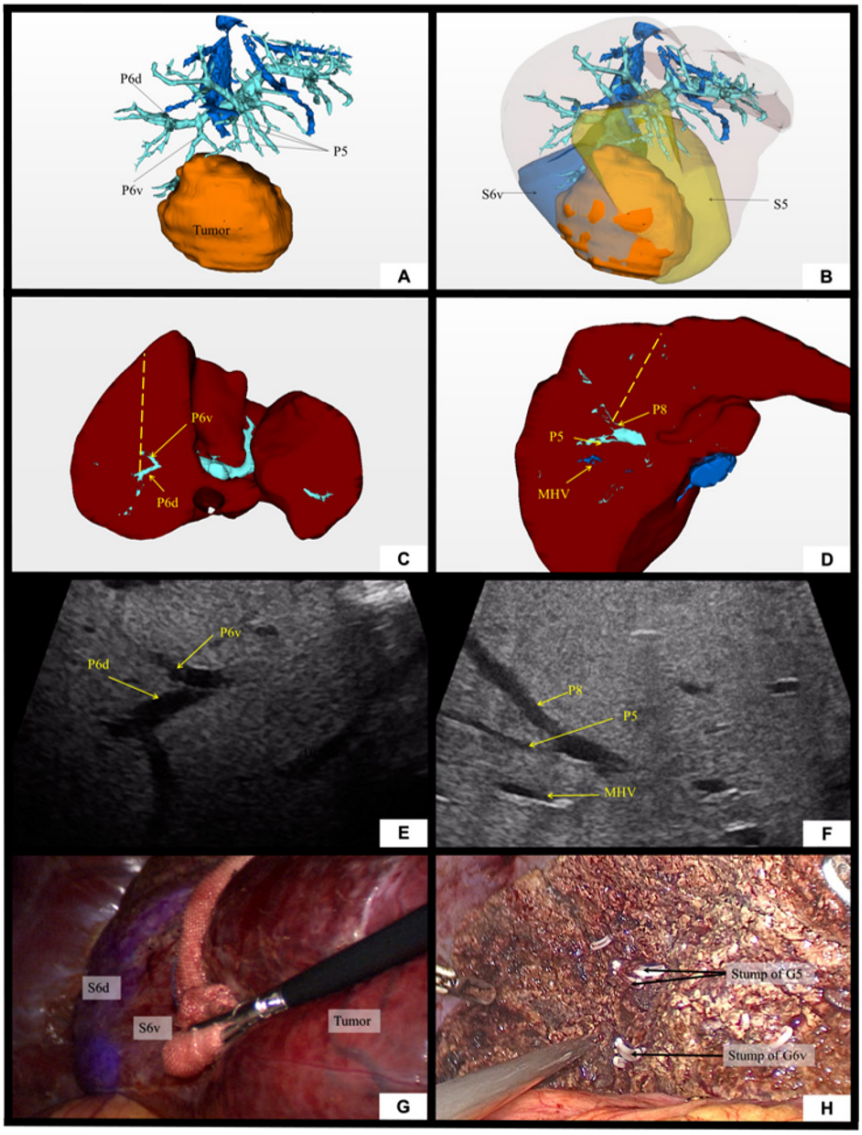

Figure 2. Counterstaining. (A,B) 3D image shows that the tumor was located in the perfusion territory supplied by the ventral branch of P6 (P6v) and P5. **(C,D)** IOUS images during the puncture of P8 and the dorsal branch of P6 (P6d) were simulated using 3D visualization technology. **(E,F)** IOUS images during the puncture of P8 and P6d. **(G)** ICG fluorescence imaging clearly shows the perfusion territory of the P6d as fluorescing, while the perfusion territory of the P6v was identified as defects in fluorescence. **(H)** Cut surface of the liver after resection of the tumor-bearing portal perfusion territory. The disconnected sections of P5 and P6v are visible in the cut surface. IOUS, intraoperative ultrasound; ICG, indocyanine green; MHV, middle hepatic vein.

unaffected (Figure 2, G and H).

2.7. Negative staining technique (Case 3)

When the tumor-bearing portal branch is temporarily clamped shut, the tumor-bearing portal territory can be recognized as a fluorescence defect *via* intravenous ICG injection (*11*). We planned LAH for a 3.8-cm-diameter HCC and ascertained from the 3D virtual image that the tumor was located at segment III (S3), segment IV (S4), and the ventral segment of the right anterior section (RASv) (Figure 3, A and B). Following the clamping of the Glisson pedicle of S3, S4, and RASv (G3, G4, G5v, and G8v) and the intravenous injection of ICG, the tumor-bearing portal territory appeared fluorescence-deficient, while the remaining areas exhibited fluorescence (Figure 3, C–F). After the resection line was marked by electrocautery, we performed LAH (Figure 3H).

2.8. Hepatectomy

We determined an effective and sustained demarcation between the prospectively removed hepatic territory and the remaining hepatic territory following ICG fluorescent liver-segment staining. Inflow was intermittently occluded using the Pringle maneuver, and the liver parenchyma was dissected using the forceps clamp-crushing technique. The orientation of the cut relative to the liver parenchyma was adjusted through manipulation under real-time guidance of IGFI. A drainage tube was subsequently placed at the hepatic transection site to monitor postoperative bleeding and bile leakage.

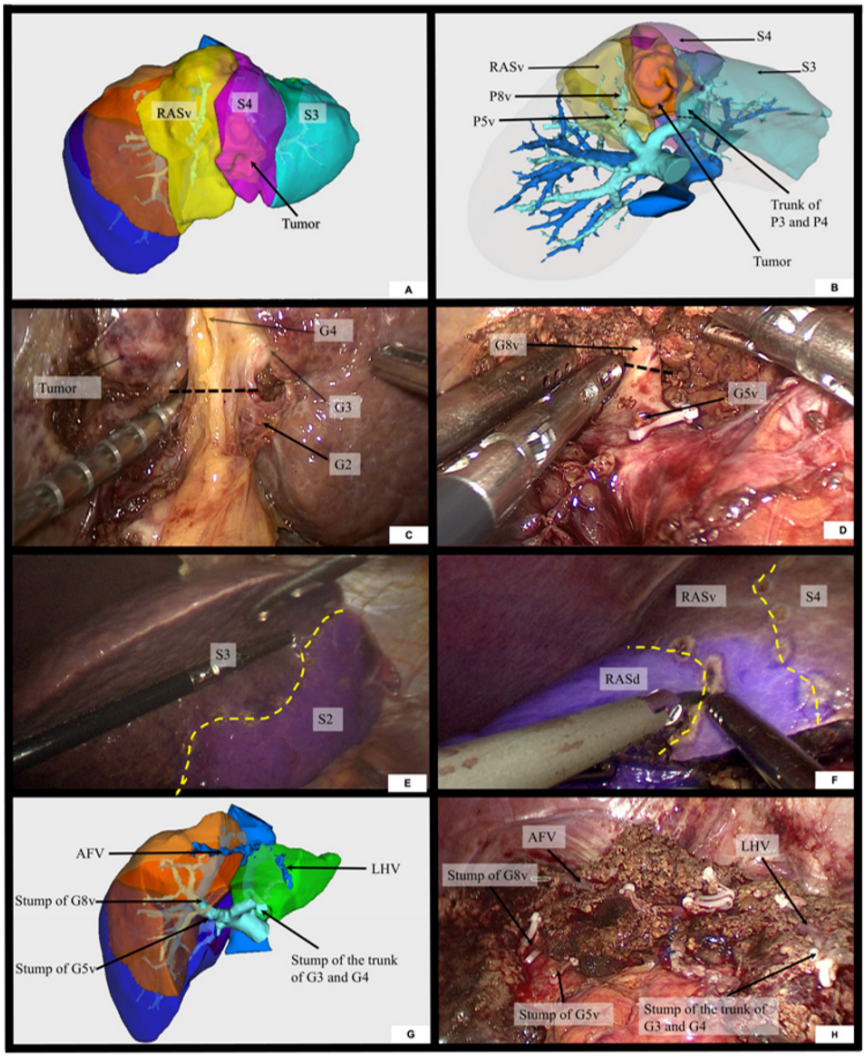

Figure 3. Negative staining. (A) 3D image shows that the tumor was located in the S3, S4, and RASv. **(B)** Access for dissection and clamping of P5v, P8v, and the trunk of G3 and G4 using 3D visualization technology. **(C)** Clamping of the trunk of G3 and G4. **(D)** Clamping of P5v and P8v. **(E,F)** After intravenous injection of ICG, S3, S4, and RASv showed fluorescence-deficient areas, and the demarcation lines on the liver surface highly resembled the boundaries on the 3D images. **(G,H)** The transection after LAH exhibited strong similarity to the transection on the 3D image after VH. ICG, indocyanine green; RAS, right anterior section; AFV, anterior fissure vein; LHV, left hepatic vein.

2.9. Follow-up

Biochemical indicators such as blood count and liver function were regularly evaluated after surgery, and an abdominal CT examination was performed approximately 3 days postoperatively to assess postoperative complications. Based on the patient's CT data, the 3D virtual image of the postoperative liver was reconstructed, and the actual remnant liver volumes (ARLVs) were calculated. ARLV and PRLV were then compared to assess the consistency of LAH versus VH.

2.10. Statistical analysis

We used proportions to summarize the distribution of categorical variables. For continuous variables, we calculated and used medians and interquartile ranges. The correlation analysis between ARLV and PRLV was conducted using Pearson's method. All statistical analyses were performed by adopting the Statistical Package for Social Sciences software, version 25.0 (IBM, Chicago, IL, USA). A p-value of < 0.05 was considered statistically significant.

3. Results

Of the 73 patients who demonstrated a valid demarcation by IGFI, 14 (19.2%) underwent hemi-hepatectomy, while 19 (26%) and 40 (54.8%) underwent sectionectomy and segmentectomy, respectively. The tumor-bearing portal territory was identified through positive staining in 22 cases, counterstaining in one case, positive staining with counterstaining in two cases, and negative staining in 48 cases. The ICG fluorescence boundaries that represented the tumor-bearing portal territory versus the normal liver could be clearly observed intraoperatively in all patients. The intraoperative IGFI-identified hepatic segment boundaries matched the boundaries of the tumor-bearing

Table 2. Summary of characteristics of patients

Characteristics	Values
Total number	73
Fluorescence staining technique	
Positive staining technique, *n* (%)	22 (30.1)
Counter staining technique, *n* (%)	1 (1.4)
Positive staining with Counter staining technique, *n* (%)	2 (2.7)
Negative staining technique, *n* (%)	48 (65.8)
Surgical procedure	
Mono-segmentectomya[a], *n* (%)	30 (41.1)
Combined-segmentectomya, *n* (%)	10 (13.7)
Sectionectomy, *n* (%)	19 (26)
Hemi-hepatectomy, *n* (%)	14 (19.2)
Operation time, median [IQR], min	355 [225–457]
Estimated blood loss, median [IQR], mL	200 [100–400]
Transfusion	
Concentrated red blood cell, median (range), U	0 (0–4)
Fresh frozen plasma, median (range), mL	0 (0–600)
Postoperative length of stay, median [IQR], day	9 [7–11]

[a] Including the removal of portal vein territory smaller than Couinaud segment. IQR: interquartile range.

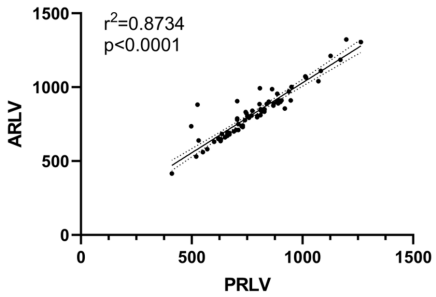

Figure 4. ARLV showed a strong correlation with the PRLV (r^2 = 0.8734, p < 0.001). ARLV, predicted remnant liver volume; PRLV, actual remnant liver volumes.

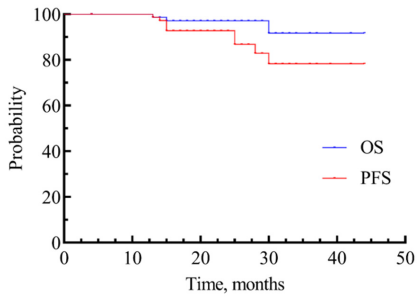

Figure 5. Kaplan-Meier curves for OS and PFS in all patients. OS, overall survival; PFS, progression-free survival.

portal territory detected by 3D visualization in 72 (98.6%) patients. Of the 22 cases in which portal injection was performed, hepatic tissues from one case (4.5%) did not stain as expected, and the stained area did not adequately cover the liver segment to be removed. We determined the target liver-segment boundaries intraoperatively by preoperative 3D virtual images combined with IOUS. LAH was ultimately completed in all cases, except for three cases in whom the conversion to laparotomy was abrogated due to massive intraoperative bleeding (Table 2 summarizes the intraoperative and postoperative results of 3D visualization-guiding ICG fluoroscopic staining for LAH).

None of the patients experienced intraoperative adverse incidents associated with ICG or fluoroscopic staining procedures. The median operative time was 355 min (interquartile range, 225–457 min), and the median estimated blood loss was 200 mL (interquartile range, 100–400 mL). All patients were discharged without major complications, and all pathologic results showed a negative resection margin. The median postoperative length of stay was 9 days (interquartile range, 7–11 days). As shown in Figure 4, ARLV and PRLV exhibited a robust correlation (r^2 = 0.8734, p < 0.0001) (Figure 4).

The median follow-up time for all patients was 22 months (interquartile range, 16–29.5 months). Survival rates at 1, 2, and 3 years were 98.6%, 97.1%, and 91.7%, respectively, while PFS rates at 1, 2, and 3 years were 98.6%, 92.8%, and 78.3%, respectively (Figure 5).

4. Discussion

Identification of portal territory by portal injection of dye under IOUS guidance constitutes an essential method for performing anatomic hepatectomy (*8*). By using this technique, the stained area is visualized on the surface of the liver. However, the intersubsegmental plane is impossible to follow when the liver parenchyma is divided, as conventional dyes fade immediately after injection (*20*). The other method widely used for anatomic hepatectomy is the Glisson pedicle approach described by Takasaki *et al*. (*9*). After the Glisson pedicle of the target liver segment is dissected and clamped, hepatic segment boundaries can be identified by the hepatic surface ischemia line. However, similar to portal staining, the Glisson pedicle approach also fails to identify the intersegmental plane during parenchymal dissection. The application of the IGFI technique can resolve these issues. Unlike conventional dye, ICG does not fade rapidly after injection and is retained by the liver for several hours (*21*). Thus, the IGFI technique enables the identification of intersegmental planes during parenchymal transection and real-time navigation in anatomic hepatectomy.

The accurate identification of target portal branches by IOUS guidance is critical for successful staining, and the preoperative clarification of the anatomic relationship between HCC and the surrounding portal vein branches is vital for the accurate identification and puncture of the target portal branch under IOUS guidance. Nevertheless, the type and number of tertiary portal vein branches in each patient vary. In 33–70% of cases, an individual Couinaud segment is supplied by two or more third-order portal vein branches (*22,23*), and a tumor may also have two or more tumor-bearing portal vein branches. This situation greatly complicates identification of the

tumor-bearing portal vein branch under IOUS guidance. Traditional 2D imaging data do not objectively reflect the complicated anatomic structure of the liver and the detailed morphologic characteristics of a lesion. Thus, accurate preoperative identification of the portal vein branch of the hepatic segment and the tumor-bearing portal vein branch using traditional 2D imaging data is quite difficult.

Using 3D virtual imaging, surgeons can observe the size, location, and morphology of the tumor and the intrahepatic vascular anatomy from different angles. This modality also allows individual segmentation of the liver by calculating the portal territory, determining the liver segment where the tumor is located, identifying the tumor-bearing portal branch, and performing surgical planning by virtual hepatectomy. Thus, 3D virtual imaging provides an anatomic basis for finding the target portal branch intraoperatively. We herein determined the locations of tumors and the identification of tumor-bearing portal branches in each patient by applying 3D virtual imaging technology. However, the IOUS image is 2D and cannot be directly matched with the 3D virtual image so as to precisely identify the target portal vein. Therefore, we simulated the IOUS image by transecting the 3D virtual image to assist surgeons in accurately identifying the target portal vein branch under IOUS (Figure 1, C and D). We were able to generate an ultrasonographic image that matched the simulated image when performing IOUS so as to quickly identify the target portal branch and perform the puncture (Figure 1, E and F). As a result, we achieved a 96% staining success rate in cases where we injected ICG into the hepatic portal vein. Therefore, preoperative, 3D virtual image-based surgical planning and simulated IOUS imaging contribute to the success of IOUS-guided portal vein injection and the precise execution of anatomic hepatectomy. The application of IOUS in laparoscopic surgery is limited by the position and angle of the trocar, and the utilization of the puncture needle is limited by the abdominal wall and the inflexibility of instruments. Therefore, the identification and puncture of the portal vein under IOUS in laparoscopic hepatectomy are more technically challenging. We recommend that these factors be taken into account when planning intraoperative IOUS-guided portal puncture *via* 3D virtual imaging preoperatively. After a successful puncture, the speed of the dye injection needs to be controlled, because rapid injection tends to cause dye reflux and staining failure.

Compared with other methods, negative staining is easier to perform in LAH. It does not require a puncture of the target portal branch but is performed by the intravenous injection of ICG after clamping the segmental portal pedicle. However, the Glisson approach is also invasive and technically demanding, particularly when the origin of the tumor-bearing portal branch is located within the liver parenchyma. 3D virtual imaging allows surgeons to understand the course of the tumor-bearing portal branch preoperatively and plan access to this portal branch, thus contributing to a reduction in the difficulty of dissection and the clamping of the target Glisson pedicle (Figure 3, C and D). Negative staining is often applied in anatomic hemi-hepatectomies and lobectomies, and such extensive hepatectomies reflect a potential to result in insufficient remnant liver volume. Since postoperative liver failure and morbidity are known to be influenced by remnant liver volume (*24*), accurate preoperative assessment of the remaining liver volume is crucial for the safe performance of anatomic hepatectomy. The PRLV was calculated after VH, facilitating preoperative assessment and reducing the incidence of postoperative liver failure and mortality. We also calculated the ARLVs postoperatively and uncovered a significant correlation between ARLVs and PRLVs. Our data therefore supported our contention that 3D virtual imaging technology enabled accurate prediction of the anatomic hepatectomy plan and indirectly demonstrated that the intraoperative volume of the resected liver was also approximately the same as the volume of the tumor-bearing portal territory in the 3D virtual images.

There were some limitations to this study. First, we had no control group, and it was thus impossible to depict differences in clinical outcomes. Additional studies are also required with respect to evaluating the differences in operative time, blood loss, disease-free survival, and mortality rates for anatomic hepatectomy with or without 3D virtual imaging and IOUS guidance. Second, the 3D virtual images could not be navigated in real time during LAH. Thus, although preoperatively created 3D virtual images and simulated IOUS images can provide a reference for liver surgeons during LAH, they cannot be matched with IOUS images and surgical views in real time. The position of the intraoperative ultrasound needs to be adjusted several times until the ultrasound image matches the preoperative simulated image. We posit that the technically complete integration of 3D visualization software with IOUS and laparoscopic systems for the real-time navigation of 3D visualization software during surgery will facilitate LAH with increased precision.

In conclusion, 3D virtual imaging and IOUS contribute significantly to the staining and identification of tumor-bearing portal territories and the accurate implementation of LAH. It enables surgeons to quickly and accurately locate and puncture or block the target portal vein during surgery, precisely identify the tumor-bearing portal territory, and perform laparoscopic anatomic liver resection.

Funding: This work was supported by a grant from the National Natural Science Foundation of China (82060454) and the project from the Second Affiliated Hospital of Nanchang University (2021efyC05).

Conflict of Interest: The authors have no conflicts of interest to disclose.

References

1. Wakabayashi G, Cherqui D, Geller DA, *et al.* The Tokyo 2020 terminology of liver anatomy and resections: Updates of the Brisbane 2000 system. J Hepatobiliary Pancreat Sci. 2022; 29:6-15.
2. Ho MC, Hasegawa K, Chen XP, Nagano H, Lee YJ, Chau GY, Zhou J, Wang CC, Choi YR, Poon RT, Kokudo N. Surgery for intermediate and advanced hepatocellular carcinoma: A consensus report From the 5Th Asia-Pacific Primary Liver Cancer Expert Meeting (APPLE 2014). Liver Cancer. 2016; 5:245-256.
3. You DD, Kim DG, Seo CH, Choi HJ, Yoo YK, Park YG. Prognostic factors after curative resection hepatocellular carcinoma and the surgeon's role. Ann Surg Treat Res. 2017; 93:252-259.
4. Wang C, Ciren P, Danzeng A , Li Y, Zeng CL, Zhang ZW, Huang ZY, Chen YF, Zhang WG, Zhang BX, Zhang BH, Chen XP. Anatomical resection improved the outcome of intrahepatic cholangiocarcinoma: A propensity score matching analysis of a retrospective cohort. J Oncol. 2022; 2022:4446243.
5. DeMatteo RP, Palese C, Jarnagin WR, Sun RL, Blumgart LH, Fong Y. Anatomic segmental hepatic resection is superior to wedge resection as an oncologic operation for colorectal liver metastases. J Gastrointest Surg. 2000; 4:178-184.
6. Ishii M, Mizuguchi T, Kawamoto M, Meguro M, Ota S, Nishidate T, Okita K, Kimura Y, Hui TT, Hirata K. Propensity score analysis demonstrated the prognostic advantage of anatomical liver resection in hepatocellular carcinoma. World J Gastroenterol. 2014; 20:3335-3342.
7. Dong J, Yang S, Zeng J, *et al.* Precision in liver surgery. Semin Liver Dis. 2013; 33:189-203.
8. Makuuchi M, Hasegawa H, Yamazaki S. Ultrasonically guided subsegmentectomy. Surg Gynecol Obstet. 1985; 161:346-350.
9. Takasaki K. Glissonean pedicle transection method for hepatic resection: A new concept of liver segmentation. J Hepatobiliary Pancreat Surg. 1998; 5:286-291.
10. Yang J, Tao HS, Cai W, Zhu W, Zhao D, Hu HY, Liu J, Fang CH. Accuracy of actual resected liver volume in anatomical liver resections guided by 3-dimensional parenchymal staining using fusion indocyanine green fluorescence imaging. J Surg Oncol. 2018; 118:1081-1087.
11. Kobayashi Y, Kawaguchi Y, Kobayashi K, Mori K, Arita J, Sakamoto Y, Hasegawa K, Kokudo N. Portal vein territory identification using indocyanine green fluorescence imaging: Technical details and short-term outcomes. J Surg Oncol. 2017; 116:921-931.
12. Simpson AL, Geller DA, Hemming AW, Jarnagin WR, Clements LW, D'Angelica MI, Dumpuri P, Gönen M, Zendejas I, Miga MI, Stefansic JD. Liver planning software accurately predicts postoperative liver volume and measures early regeneration. J Am Coll Surg. 2014; 219:199-207.
13. Li PP, Wang ZH, Huang G, Huang ZP, Li Y, Ni JS, Liu H, Fang CH, Zhou WP. Application of liver three-dimensional visualization technologies in the treatment planning of hepatic malignant tumor. Zhonghua Wai Ke Za Zhi. 2017; 55:916-922. (in Chinese)
14. Saito S, Yamanaka J, Miura K, Nakao N, Nagao T, Sugimoto T, Hirano T, Kuroda N, Iimuro Y, Fujimoto J. A novel 3D hepatectomy simulation based on liver circulation: application to liver resection and transplantation. Hepatology. 2005; 41:1297-1304.
15. Takamoto T, Hashimoto T, Ogata S, Inoue K, Maruyama Y, Miyazaki A, Makuuchi M. Planning of anatomical liver segmentectomy and subsegmentectomy with 3-dimensional simulation software. Am J Surg. 2013; 206:530-538.
16. Urata K, Kawasaki S, Matsunami H, Hashikura Y, Ikegami T, Ishizone S, Momose Y, Komiyama A, Makuuchi M. Calculation of child and adult standard liver volume for liver transplantation. Hepatology. 1995; 21:1317-1321.
17. Belgihiti J, Clavien PA, Gadzijev E, Garden JO, Lau W, Makuuchi M, Strong RW. The Brisbane 2000 terminology of liver anatomy and resections. HPB. 2000; 2:333-339.
18. Clavien PA, Barkun J, de Oliveira ML, Vauthey JN, Dindo D, Schulick RD, de Santibañes E, Pekolj J, Slankamenac K, Bassi C, Graf R, Vonlanthen R, Padbury R, Cameron JL, Makuuchi M. The Clavien-Dindo classification of surgical complications: Five-year experience. Ann Surg. 2009; 250:187-196.
19. Takayama T, Makuuchi M, Watanabe K, Kosuge T, Takayasu K, Yamazaki S, Hasegawa H. A new method for mapping hepatic subsegment: counterstaining identification technique. Surgery. 1991; 109:226-229.
20. Sakairi T, Makuuchi M. Identification of the intersegmental or subsegmental plane in the liver with a surgical clip. Surgery. 1991; 110:903-904.
21. Xu Y, Chen M, Meng X, Lu P, Wang X, Zhang W, Luo Y, Duan W, Lu S, Wang H. Laparoscopic anatomical liver resection guided by real-time indocyanine green fluorescence imaging: experience and lessons learned from the initial series in a single center. Surg Endosc. 2020; 34:4683-4691.
22. Kogure K, Kuwano H, Fujimaki N, Ishikawa H, Takada K. Reproposal for Hjortsjo's segmental anatomy on the anterior segment in human liver. Arch Surg. 2002; 137:1118-1124.
23. Hata F, Hirata K, Murakami G, Mukaiya M. Identification of segments VI and VII of the liver based on the ramification patterns of the intrahepatic portal and hepatic veins. Clin Anat. 1999; 12:229-244.
24. Schindl MJ, Redhead DN, Fearon KC, Garden OJ, Wigmore SJ; Edinburgh Liver Surgery and Transplantation Experimental Research Group (eLISTER). The value of residual liver volume as a predictor of hepatic dysfunction and infection after major liver resection. Gut. 2005; 54:289-296.

Received April 27, 2025; Revised July 31, 2025; Accepted August 6, 2025.

Released online in J-STAGE as advance publication August 10, 2025.

§*These authors contributed equally to this work.*
**Address correspondence to*:
Kai Wang, Hepato-Biliary-Pancreatic Surgery Division, Department of General Surgery, The Second Affiliated Hospital of Nanchang University, 1 Minde Road, Donghu District, Nanchang 330006, China.
E-mail: ndefy07021@ncu.edu.cn